Analysis of natural landing trajectories for passive landers in binary asteroids: A case study for (65803) 1996GT Didymos

Onur Celik[a,1,*], Joan Pau Sánchez[b,2], Ozgur Karatekin[c,3], Birgit Ritter[d,4]

[a] The Graduate University for Advanced Studies (SOKENDAI), 3-1-1 Yoshinodai, Chuo-ku, Sagamihara, Kanagawa, 252-5210, Japan, +81 (0)50 6867 5062
[b] Cranfield University, College Road, Cranfield, Milton Keynes, MK43 0AL, United Kingdom, +44 (0)1234 750111 x5120
[c] the Royal Observatory of Belgium, Avenue Circulaire 3, Uccle, Brussels, 1180, Belgium, , +32 (0)2 373 6730
[d] the Royal Observatory of Belgium, Avenue Circulaire 3, Uccle, Brussels, 1180, Belgium, , +32 (0)2 373 6753

Abstract

Binary asteroids are believed to constitute about 15% percent of the near-Earth asteroid (NEA) population. Their abundance and yet-to-be-resolved formation mechanism make them scientifically interesting, but they can also be exploited as a test bed for kinetic impactors, as the Asteroid Impact and Deflection Assessment (AIDA) joint mission proposal suggested. Due to the highly perturbed dynamical environment around asteroids, large, and generally expensive missions are preferred to be operated in a safe distance to the target asteroid. Even if advanced remote sensing techniques provide the finest details of the target, surface agents can obtain higher resolution and ground truth data even by using rather simple measurement methods. A team led by the Royal Observatory of Belgium (ROB) proposed the Asteroid Geophysical Explorer (AGEX) CubeSat to land on the smaller companion of Didymos, in response to the Asteroid Impact Mission call, as a part of AIDA proposal. This research investigates novel and purely ballistic landing trajectories for passive landers like AGEX by exploiting the natural dynamics of binary systems and their robustness. The framework of Circular Restricted Three-Body Problem (CR3BP) is used for this purpose. A newly developed bisection algorithm ensures to generate the lowest energy trajectory for landing point under given constraints. The results suggest that landing speeds less than 8 cm/s are possible, while the coefficients of restitution over 0.9 would ideally ensure a successful landing. However, robustness of trajectories is also investigated in a Monte Carlo simulation. A success rate over 99.7% (3σ) can be achieved for a wide region, though extra requirements might need to be considered for the mothership design.

Keywords: Binary asteroids, Didymos, natural landing trajectories, CR3BP, CubeSat

1. Introduction

Binary asteroids constitute a considerable portion of near-Earth asteroid population; about 15% according to recent estimates [1]. Among variety of missions proposed to asteroids, or to small bodies in general, the interest on binary asteroids also seems to grow. Within the last decade, submitted mission proposals included Marco Polo-R, Binary Asteroid in-situ Exploration (BASiX), and Asteroid Impact and Deflection Assessment (AIDA) [2, 3, 4]. However, since the first and only ever visit of Galileo spacecraft to binary asteroid Ida-Dactyl, no other mission has aimed for binaries.

Apart from scientific curiosity, and its escalating commercial value, asteroid exploration is also important for its potential impact risk to the Earth. The threat is taken seriously and a variety of techniques

---

[*] Corresponding author
   Email address: `onur.celik@ac.jaxa.jp` (Onur Celik)
[1] Research Student, Department of Space and Astronautical Science
[2] Lecturer/Assistant Professor, School of Aerospace, Transport and Manufacturing
[3] Senior Researcher, Reference Systems and Planetology
[4] Researcher, Reference Systems and Planetology

is proposed to deflect potentially hazardous asteroids. One of those is the kinetic impactor, which involves a high-speed spacecraft that is designed to crash on target asteroid in order to steer it away from its orbital path to mitigate the risk of impact [5]. Binary asteroids are ideal test beds to demonstrate capabilities of such techniques. Indeed, single asteroids are much more abundant, thus would likely be easier to target one, however it is much more challenging to observe changes in their orbit due to much longer period of motion. On the other hand, smaller companions in the binaries are orbiting their primaries in much shorter timescales; usually one or more orbits are completed less than a day. Hence, changes in an orbit after an impact would likely be much easier to observe.

The goal of the joint NASA/ESA multi-spacecraft mission proposal AIDA is to test the kinetic impactor technique in the binary asteroid (65803) 1996GT Didymos [4]. Between two spacecraft proposed, NASA spacecraft Double Asteroid Redirection Test (DART) is planned to perform a high-speed impact on the smaller companion of Didymos [4], informally called Didymoon. Whereas ESA spacecraft Asteroid Impact Mission (AIM), whose future is now uncertain, tasked to observe pre- and post-impact variations on Didymoon orbit, as well as general properties of the binary system in order to understand the formation mechanism [4]. AIM proposal also includes MASCOT-2 lander designed by German Aerospace Center, DLR and French Space Agency, CNES, to perform in-situ observations and two CubeSats to be deployed in the binary system in order to fulfill a secondary goal to test novel intersatellite communication techniques and enhance CubeSat heritage in interplanetary medium [6]. For the latter, ESA opened a call to the community in 2015 for novel CubeSat proposals [6].

As a response to the call, the Royal Observatory of Belgium (ROB) proposed two 3U CubeSats to land on Didymoon, named as Asteroid Geophysical Explorer (AGEX) mission [7]. The first spacecraft (SeisCube) in the proposed concept includes a geophysical instrument package with a seismometer and a gravimeter to investigate subsurface properties. The second spacecraft (Bradbury) in fact carries a number of femtosats to be deployed throughout the surface, which are equipped with miniaturized instruments to investigate surface properties. Additionally, both CubeSats also accommodate same set of sensors in order to measure rotation and surface mechanical properties of Didymoon [7]. The landing operation of the AGEX mission is foreseen to be fully passive, i.e. the proposed landing trajectories shall occur naturally, this is without the need of propulsive systems.

Such trajectories can be found in the Circular Restricted Three-Body Problem (CR3BP) dynamical model, in which the three bodies are the two binary companions and the lander CubeSat. In principle, these trajectories are driven only by natural dynamics, which means no active control on the trajectory is necessary. This then makes these trajectories ideal conduits for NanoSats or other small landers, that possess no, or only minimal control capabilities. It could also be a preferable solution for motherships, such as AIM, to deploy landers from a safer distance as the dynamical environment around asteroids imposes non-negligible risks to low-altitude landing operations. As a consequence, the research on delivering NanoSats, or science packages, on binary surfaces has gained a considerable interest.

Natural manifold deliveries of science packages on binary asteroid sur are studied by Tardivel and Scheeres [8]. They considered the vicinity of Lagrange points as deployment locations and defined first intersection of a trajectory with surface as landing [8]. This work followed a strategy development for landings in binary asteroid 1996 FG3, back-up target of Marco Polo-R mission proposal [9]. In a Monte Carlo analysis, they assessed the statistical success of landings [9]. Moreover, within the context of MASCOT-2 lander, Tardivel et al. [10] discussed the passive landing opportunities on Didymoon, later with an additional optimization study carried out by Tardivel [11]. Along the same line, Ferrari carried out a trajectory design and Monte Carlo uncertainty simulation for MASCOT-2 [12]. The study offers a landing strategy for ballistic landing based on Poincaré maps with special emphasis on AIM proposal [12]. In a recent study, Celik and Sánchez proposes a new technique to seek for opportunities for ballistic soft landing in binary asteroids [13]. This technique defines a landing in local vertical and utilizes a bisection search algorithm to search minimum energy trajectories in a backwards propagation from the surface. In similar contexts, post-touchdown motion on asteroids is also tackled by several researchers [14, 15, 16].

In the context of ROB's AGEX proposal, and on the groundwork of Celik and Sánchez, this paper focuses on a robustness analysis of ballistic landing for a CubeSat lander targeting Didymoon, under uncertainties and GNC errors by means of a Monte Carlo simulation. A spherical shape and point mass gravity are assumed for both binary companions, Didymain and Didymoon. A dense grid of landing points are created and distributed homogenously on the surfaces of the companions, whose locations are described by their latitudes and longitudes. Trajectories are then generated from each point by applying the methodology developed in [13]. This allows us to obtain nominal trajectories under ideal conditions, as well as to generate an overview of reachable regions and characteristics of landings on

the surface as a function of landing location.

Unlike previous body of work, which is restricted to trajectories emanating from near Lagrange points, the generality of the methodology here provides a complete trajectory database for ballistic landings for each point in the grid that extend beyond Lagrange points. In principle, that allows evaluating successes for all regions of interest. Readily available trajectory database also contains useful information about trajectories, such as landing speeds. Landing speeds are the only parameter that defines characteristics of a trajectory along with predefined landing locations, as a consequence of local vertical landing. Thus, they can be modified to estimate the upper limit of required energy damping, or coefficient of restitution, in order to achieve higher success rates. Moreover, deployment locations are selected as the first intersection of a landing trajectory and an artificially defined safe distance from the binary barycenter, as a representative mothership location at the time of deployment. Thus, the analyses are not restricted to a certain distance, but can be generalized to larger or shorter distances of mothership from the barycenter, for all deployment locations.

Several, realistically defined uncertainty and error sources are randomly added to nominal trajectories. After a sufficient number of test cases are propagated in a Monte Carlo simulation from corresponding deployment locations onto the surface, this paper aims to draw a preliminary conclusion about how non-ideal conditions might possibly affect touchdown success. This approach yields an overall picture of dispersion shape on the surface, as well as upper and lower boundaries for expected landing speeds, time durations and impact angles. Particularly, impact angles are treated as a simple criterion, due to definition of landings in local vertical, to assess relative robustness of trajectories. Furthermore, Monte Carlo success rates in all equatorial regions are also computed. This presents an overview about statistical success of landings in various equatorial longitudes under the assumptions provided. Finally, the paper also attempts to identify major error sensitivity sources that have an impact on touchdown success and suggestions to mitigate them.

2. Overview of Landing Trajectory Design

Suppose a mothership, in its operational orbit, orbiting at a safe distance from the binary systems barycentre. A passive lander (or a NanoSat) can be sent onto the surface of one or the other binary companion from this mothership by exploiting the natural dynamics around the binary system. Landing trajectories in this dynamical scheme can be designed in the framework of Circular Restricted Three-Body Problem (CR3BP). In this framework, the third body (i.e. the lander) moves under the gravitational attraction of its primary and secondary (i.e. Didymain and Didymoon) by having only negligible effect in return. The dynamical model is traditionally derived in the rotational frame, whose center is at the barycenter of larger bodies, x-axis is on the line connecting them and z-axis pointing the normal of their mutual orbit plane [17]. Therefore, unless otherwise stated, the models and results will be provided in the rotational barycentric reference frame. CR3BP exhibits five equilibria, called Lagrange points (L1-L5), and five different regimes of motion, expressed in zero-velocity surfaces (ZVS) [17]. For our notional mothership, an operational orbit can be defined in the exterior realm of ZVS, in which the L2 point is closed so that no natural motion is allowed to the interior realm. In this setting, L2 point presents the lowest energy gate to reach the interior region. Thus, a simple spring mechanism available on a mothership can provide a gentle push to increase the lander's energy in order to open up ZVS at L2 point and allow the motion to interior.

The problem of landing trajectory design in such a scenario is tackled in the groundwork study performed by Celik and Sánchez in the context of a hypothetical binary asteroid, whose shapes are spherical and properties are a good representation of known near-Earth binary asteroid population [13]. In this study, a landing is defined in the local vertical of a landing site, described by its latitude and longitude. Such description had the clear advantage of describing landing by only one parameter, i.e. landing (or touchdown) speed, $v_{landing}$, once a specific landing location is determined. Those initial state vectors are then propagated backwards from the surface to exterior region of ZVS in a specially developed bisection algorithm, inspired by Ren and Shan [18]. The algorithm searches for minimum energy landings in a reverse-engineered, iterative manner from the surface to exterior region of ZVS. This simple algorithm then allows trajectories to be designed for any arbitrary latitude–longitude pairs on the surface for any size of binary asteroids. Thus, it generates an overall picture for various features of landing, namely energies, speeds and coefficient of restitution (*CoR*) values. Moreover, after resulting trajectories are propagated sufficiently long time, multitudes of deployment points can be found on the path, for trajectory portions whose positions are beyond L2 point. As a result, maneuver velocities to decrease the energy below L2 point can also be computed for each point. Note that this maneuver

velocity is computed in backwards integration, and therefore corresponds to an energy increase in forward propagation to allow the motion to reach the interior region from L2 point. It should be noted, that although spherical binary asteroid pairs are used, the methodology is general and can be applied to asteroids of any shape, in fact for all small bodies, as done for Philae's descent trajectory computation [19].

A simulation was carried out with the algorithm, explained in the preceding paragraph, for landings in Didymoon. The physical properties of Didymos system is provided in Table 1. The results of landing speeds are provided in Fig. 1. The Jacobi constant (i.e. energy) results are found to be less relevant to the analyses later, and therefore not provided.

Table 1: **Properties of (65803) 1996GT Didymos.**

Property	Didymain	Didymoon
Diameter [km]	0.775	0.163
Density [kg/m^3]	2146	
Mass [kg]	5.23 x 10^{11}	4.89 x 10^9
Mutual orbit radius [km]	1.18	
Mutual orbit period [h]	11.9	

In Fig. 1, 0° represents the prime meridian whose point is arbitrarily defined as to be on x-axis, directly facing L2 point; thus 0° and 360° correspond to same longitude. In general, L2 facing regions exhibit lowest energy characteristics, in agreement with the results for larger hypothetical binary [13]. Landings to those regions are possible with less than 10 cm/s, with the lowest being on the order of ~5 cm/s. About the half of Didymoon surface is reachable with such low energy landings. The results show a clear symmetry in latitudinal direction, while the same is not true for longitudinal direction, due to the rotation of Didymoon around its primary. It should also be noted that a region about 30°-wide on the surface is not available for passive landings and marked as "no landing". Landings to that region are affected by the algorithm constraints, and would require to pass through the interior of Didymain. Note in Figure 1 that landing speeds higher than 1 m/s is equated to 1 m/s in order to increase the resolution of the colour map.
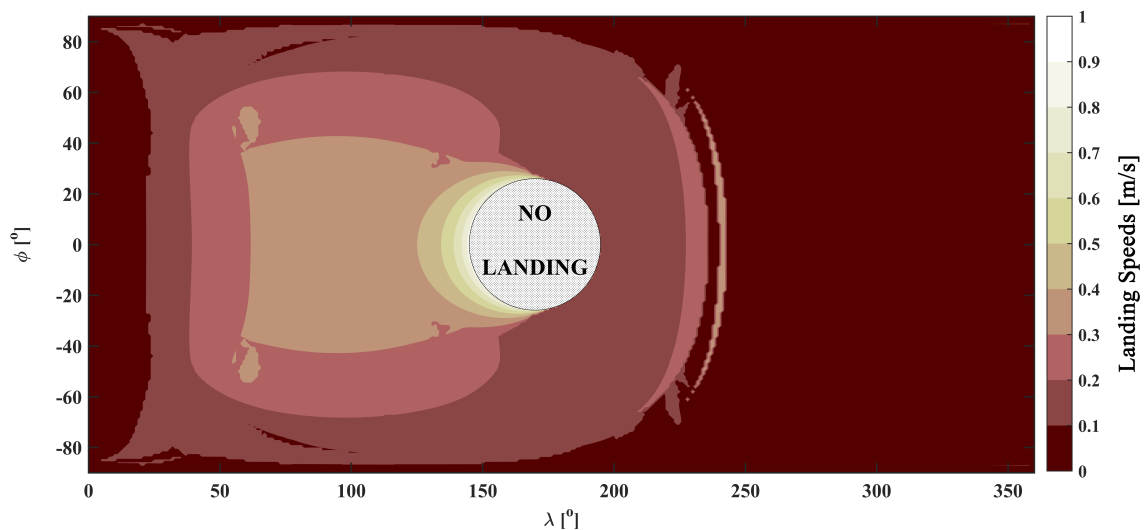
**Figure 1: Landing speeds on Didymoon surface.**

As discussed earlier, the trajectory design technique also enables us to estimate *CoR* values on the surface. *CoR* in this study refers to the simple interaction between surface and a landing spacecraft with a specific value, similar to a bouncing ball on a surface and can be described in both local vertical and local horizontal. However, this paper only concerns with *CoR* values in local vertical, and assumes that the outgoing velocity is in the same plane as the incoming velocity and the surface normal vector. This may change due to surface features, such as boulders or rocks, however that is not considered here.

CoR value then defines the energy dissipation due to surface properties, as in Eq. 1 in its simplest way.

$$\boldsymbol{v}_{LV}^{-} = (\hat{\boldsymbol{n}}.\boldsymbol{v}).\boldsymbol{v} \implies \boldsymbol{v}_{LV}^{+} = -CoR\boldsymbol{v}_{LV}^{-} \tag{1}$$

where subscripts (-) and (+) indicate incoming and outgoing speeds, respectively. *CoR* values must typically be between 0 and 1, but it may be considerably different in local horizontal and vertical directions [14, 20].

We can now compute *CoR* values to close ZVS at L2 point for landings depicted in Fig 1. Basically, this is a rough estimate of how much energy needs to be dissipated in a touchdown, so that motion of a lander (or a CubeSat) would be trapped near the binary system. It is clear that the same computation can also be performed for L1 and in fact the motion can be trapped around Didymoon, but our goal is to find the minimum dissipation necessary. Then, unless otherwise stated, *CoR* will always refer to the required energy dissipation to reduce the energy below that of L2 point. The results are provided in Fig. 2.
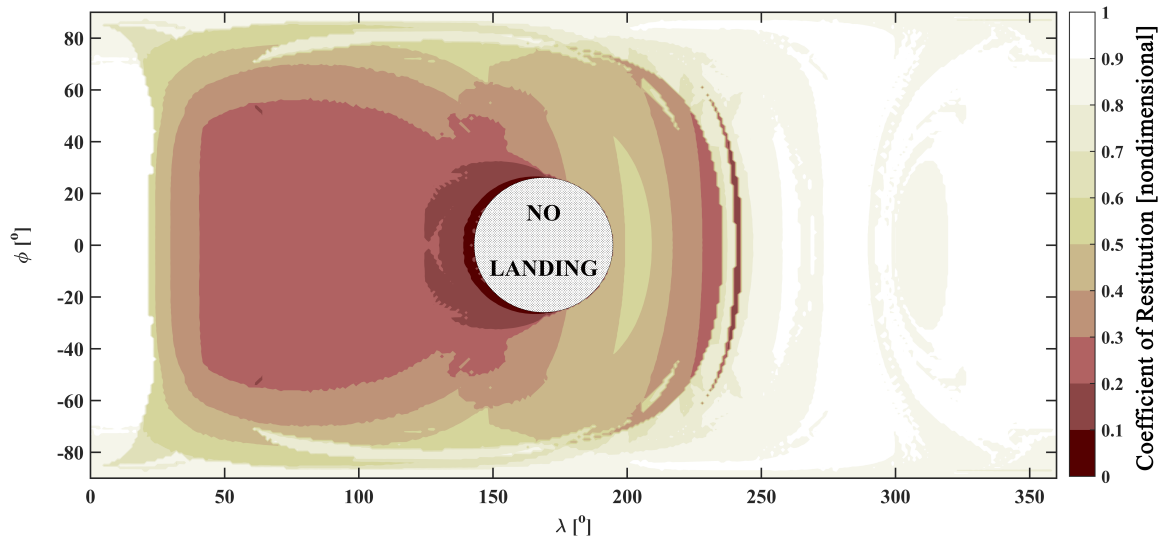
Figure 2: Required energy damping (*CoR*) to close ZVS at L2 point.

In a clear agreement with the results in Fig. 1, low energy regions show higher *CoR* values, hinting that very little energy dissipation would be enough to keep a lander near the binary system. In higher energy regions, *CoR* values begin to decrease to levels, for which a lander would likely to require an active landing system. Thus, for a purely passive landing, regions with low landing speed and high *CoR* appear to be more attractive options to consider. The focus of this study will therefore be those regions, even though results for other regions will also be presented. Hence, the values computed are essential to analyses in upcoming sections. For more detailed discussion about the results in Fig. 1 and 2, the reader may refer to the original work of Celik and Sánchez, or various others [13, 14, 15, 16, 20, 21].

Overall, although trajectories show a compelling prospect to be utilized as a landing strategy, their robustness is still in question. Particularly, trajectories are generated by this algorithm are largely idealized with relatively ad-hoc constraints [13], and it is thus necessary to assess their robustness against non-ideal conditions.

3. Robustness Analysis: Monte Carlo Simulation

The generated nominal trajectories show promising landings for the CubeSat. However, most of low energy trajectories spend some time around L2 point before a touchdown. Then the question arises about their robustness against non-ideal conditions. A convenient way to test this is a Monte Carlo simulation, in which a large number of randomly generated samples is used to understand the overall statistical behavior of a system. Here, a Monte Carlo simulation is set up to assess the robustness of these trajectories, especially for those requiring lower energies. The simulation is restricted to equatorial landing trajectories (i.e. 2D).

3.1. Trajectory refining from the database

The nominal trajectory database is used to refine trajectories that are going to be used for Monte Carlo simulation. The trajectory information shown in Fig. 1 and 2 are obtained from 4 Didymos period simulations, i.e. about 2 days. This is a rather long term for landing operations, especially provided the fact that the CubeSat is unpowered and dynamical environment is highly uncertain. Thus, 12-h (i.e. one Didymos period) trajectory information is considered to be sufficient. This condition is established as the first criterion in the trajectory refining process.

The second criterion is the minimum deployment altitude. Clearly, if the deployment altitude is lower, the landing (or at least, touchdown) success will likely be higher. However, lower altitudes are rather unfavorable locations, where non-homogenous gravitational field of the Didymos system is more effective, and also close to the dynamically unstable equilibrium point, L2. Bringing a mothership to this region might impose serious risks to mission operations. Hence, a minimum close approach distance is defined for the mothership, whose radius is measured from the barycenter along the x-axis as

$$r_{d,min} = d_{barycentre-moon} + r_{moon} + d_{safe} \qquad (2)$$

where $r_{d,min}$ in Eq. 2 is the mothership orbit radius, $d_{barycentre-moon}$ is the distance from barycenter to Didymoon centre of mass, r_{moon} is Didymoon radius and d_{safe} is the safe distance for the mothership from the barycentre, which is a parameter that will be controlled. d_{safe} is selected 200 m as the minimum deployment altitude as for the initial analysis. Even though this altitude still seems close to the surface, it is beyond the L2 point of the system, hence can be deemed as relatively safe. A similar reasoning is also made during MASCOT-2 landing analysis [22]. The minimum close approach radius for the mothership, $r_{d,min}$, then adds up to 1451.6 m from the barycenter.

The first intersection of a trajectory with $r_{d,min}$ is considered to be the deployment location. It may happen that there could be other intersections over the course of one trajectory simulation, but they are simply neglected. Note that the choice of the first intersection (i.e. closest deployment location to the surface) results in different deployment altitudes based on the target longitude, when measured from the surface of Didymoon.

Above two criteria were initially applied to the trajectory database to extract possible deployment locations for various landing locations (defined by longitudes). Especially in the low energy regions, which are more of our interest, touchdown duration is much longer than 12 h from the closest approach distance of the mothership, d_{safe}. As a result, less deployment opportunities exist with the above two criteria. Thus, if energy of trajectories can be increased, or in other words, if higher speeds can be tolerated in touchdown, faster trajectories can be obtained. This would be possible with an increase in landing speeds. A third criterion can then be defined in order to scale the speeds up in the surface:

$$v_{landing} = \frac{v_{L2}}{CoR} \qquad (3)$$

where $v_{landing}$ is landing speed (i.e. resulting speed after the bisection search), v_{L2} is the necessary speed at a landing location to close L2 point to restrict the motion to interior realm and CoR is coefficient of restitution. v_{L2} is smaller than $v_{landing}$ by definition, hence using v_{L2} in the scaling process makes our CoR even more conservative. For instance, the landing speed $v_{landing}$ for 0° longitude is 5.81 cm/s, and v_{L2} is 5.36 cm/s. When the latter is substituted in Eq. 3 to scale up $v_{landing}$ with a $CoR = 0.7$ assumption, the new landing speed becomes 7.66 cm/s. Consequently, it becomes as if the CoR value equals to ~0.75 if the nominal $v_{landing}$ value would have been used in Eq. 3, instead of v_{L2}.

Fig. 2 shows that in the L2-facing region, coefficient of restitution values may be higher than 0.9 for simple bouncing motion assumption. This is a very conservative, and possibly rather inaccurate estimation, in comparison to previous results obtained for the asteroid Itokawa (~0.85) [23], and the comet 67P/Churyumov-Gerasimenko (~0.7) [21]. The studies for MASCOT-2 landing also considered values as low as 0.6 or even lower [22]. Hence, a CoR value of 0.7 is found to be conservative enough for this study. This value is then substituted in Eq. 3 to scale landing speeds. The value seems rather arbitrary; however, it is in the lower range of observed values in small bodies, and higher than the values considered for the MASCOT-2 landing analyses.

This new CoR value is fixed everywhere in the equatorial region. It is obvious that CoR values differ across the surface. Furthermore, there is also a region in Fig. 2, exhibiting much lower CoR values than 0.7, even lower than the value used for the MASCOT-2 landing analyses (~0.6) [22]. It means that, by recomputing their $v_{landing}$ with $CoR = 0.7$, their energies are actually decreased. It is likely that some of the previously available deployment options will disappear for some of those longitudes. Although the results for those will also be provided, those are not our major regions of interest, since a landing to

6

those would potentially require powered or semi-powered landers. We will restrict our attention to those that provide low energy, passive landing prospects.

The choice of *CoR* = 0.7 makes trajectories remarkably faster and generally available for the first intersection within 12-h simulation. As an example, the trajectory targeting the prime longitude (i.e. 0°), takes ~1.2 h to reach the first intersection. Before *CoR* modification, recall that the trajectory did not have enough energy to reach the same point within 12 h.

Finally, a fourth criterion comes from the preceding study [13] and sets an upper bound of 2 m/s for maximum possible deployment speed. This upper bound is due to readily available technology for standardized CubeSat deployers [24].

Then, the criteria formulated above can be summarized below:

- Release location must be searched within 12-h (one Didymos orbit) simulation time from the surface.

- d_{safe} must be no lower than 200 m altitude.

- Landing speeds need to be scaled up according to an expected *CoR* of 0.7.

- Maximum deployment speed must not exceed 2 m/s.

Consequently, trajectories that satisfy above criteria in the backwards propagation are selected for Monte Carlo simulation. Pseudo-random uncertainties and errors, that will be described in the next subsection, are then added to the refined trajectories to run forwards from the deployment location, i.e. the first intersection of trajectories with the closest approach distance of the mothership, $r_{d,min}$.

3.2. Uncertainty and error sources

The uncertainty and error sources and their corresponding values can now be described. Those mothership- and spring-related errors and Didymoon density uncertainty. The mothership-related uncertainties are restricted to GNC errors, namely orbit determination errors in position and velocity of the mothership. An uncertainty sphere is defined for each with spacecraft in the center, and whose radii are defined by their 3σ values. The spring error is described in two parts, i.e. magnitude and angular errors. The angular error in the spring vector is in azimuth (α) and elevation (α), stretching to both positive and negative direction. The resulting spring vector then must be inside a wedge, whose dimensions are described by maximum error magnitude and angles $\pm\alpha$, $\pm\phi$.

Lastly, density errors associated with the binary system are considered. Didymos total system mass is known in a reasonable accuracy, as 5.28 x 10^{11} kg [25]. However, their individual masses and densities are not known exactly. Under our spherical asteroid and same density assumptions for both asteroid bodies, this breaks down into 5.23 x 10^{11} kg for Didymain and 4.89 x 10^9 kg for Didymos, as in Table 1. As the system mass is known with a good accuracy, density uncertainty is only considered for Didymoon. However, Didymoon contribution to the total system mass is only ~1.2%, therefore it can be expected that it would not be as effective as an uncertainty in Didymain or in total system mass. Those effects simply are not considered here and left for a possible future study. Table 2 shows 3σ uncertainty and errors considered for Monte Carlo simulation.

Table 2: Uncertainty and error sources.

Source	3σ value
GNC position accuracy	15 m
GNC velocity accuracy	0.5 cm/s
Spring magnitude error	±30%
Spring angle error	±15°
Didymoon density uncertainty	±30%

Additionally, solar radiation pressure is found to have a negligible effect on trajectories, mostly due to the short duration of landing. Its effect is on the order of a millimeter in position and 10^{-4}–10^{-5} mm/s in velocity.

Apart from the mentioned uncertainties and perturbations; surface properties, mass distribution, the exact shape of Didymoon and some other perturbations will certainly have an impact on touchdown location and velocities. However, these are simply not considered in this study. With regards to the

shape, note that only epistemic uncertainties in the shape of the asteroid (i.e. inaccuracies on the final shape model) will affect the feasibility of the landing trajectories. In other words, the same procedure implemented here can be used with a more realistic shape model for Didymos, once this is known. Thus, only the errors in the final shape model will actually affect the trajectories, not the fact that at this stage a spherical shape is considered.

3.3. Simulation model

The Monte Carlo simulation model used here can be explained in three parts: first, refining trajectories from the database, second, generating pseudo-random uncertainty and error added trajectories, and third, trajectory propagation. Trajectory refining and uncertainty and error sources are explained in the previous two subsections. This section will discuss on how uncertainty- and error-added trajectories are generated from refined trajectories, effects of individual sources, and simulation model in general.

One of the advantages of reverse-engineered landing trajectories is their compact nature, providing a landing velocity vector on the surface. Then, after the bisection search, the resulting trajectory provides deployment velocities at possible deployment locations above the surface. This vector in reality is the sum of mothership orbital velocity and deployment spring velocity, as in Eq. 4, below:

$$\boldsymbol{v}_{deployment} = \boldsymbol{v}_{SC} + \boldsymbol{v}_{spring} \tag{4}$$

Here, $\boldsymbol{v}_{deployment}$ is the deployment velocity, $\boldsymbol{v}_{SC}$ is the mothership velocity and $\boldsymbol{v}_{spring}$ is the spring velocity.

Eq. 4 then allows us to consider and evaluate mothership- and spring-related uncertainties and errors separately, which would otherwise be rather difficult, and impossible to see their individual impacts on landing success. However, here we have an underdetermined problem with one known vector ($\boldsymbol{v}_{deployment}$), and two unknown vectors. Thus, in order to treat them individually, it is necessary to know or assume either $\boldsymbol{v}_{SC}$ or $\boldsymbol{v}_{spring}$, in addition to $\boldsymbol{v}_{deployment}$. It seems clear that $\boldsymbol{v}_{SC}$ is an easier target to make assumptions. The deployment operation will likely to include a close approach of the mothership in a hyperbola in barycentric inertial frame. In the closest approach, this can be translated as an instantaneous velocity in +y direction in rotational frame, due to an epicycle near L2 point, as also described in [11]. Assuming that the mothership will perform the deployment in the instant of the closest approach, $\boldsymbol{v}_{SC}$ can be defined by only assuming one parameter, i.e. velocity in +y direction in co-rotating frame, and whose magnitude is assumed as 2 cm/s. Then, Eq. 4 can be written in following form to estimate the spring velocity, $\boldsymbol{v}_{spring}$:

$$\boldsymbol{v}_{spring} = \boldsymbol{v}_{deployment} - \boldsymbol{v}_{SC} \tag{5}$$

It is usually more difficult to design a definite spring velocity, as landing location is defined as a region rather then a target point. This shows yet another useful feature of reverse engineering: as landing velocity is defined for a certain landing location, then above Eq. 5 computes the spring velocity for that point. This then provides an accurate estimate of spring velocities for each landing point. If there is a landing region defined instead of a landing point, spring velocities for each landing point inside that region can easily be obtained, thus maximum tolerable errors in landing operations.

After obtaining $\boldsymbol{v}_{spring}$, uncertainties and errors are going to be added to $\boldsymbol{v}_{spring}$ and $\boldsymbol{v}_{SC}$ to estimate the new deployment velocity that deviate from the nominal deployment velocity, defined as below:

$$\boldsymbol{v}_{deployment,u} = \boldsymbol{v}_{SC,u} + \boldsymbol{v}_{spring,u} \tag{6}$$

The subscript u in Eq. 6 is used to distinguish nominal trajectory from uncertainty- and error-added, deviated trajectories.

The uncertainties and errors are then inputted to a trajectory in a pseudo-random way, i.e. a randomly selected value is seeded for each trajectory from each bounded set of sources. For each set of propagation, 1000 trajectories are generated by adding uncertainties and errors to nominal trajectories. Those are then propagated in forward time to the surface from the deployment location. A sufficient propagation time is allowed and an event function in the program is used to mark a touchdown.

The success criterion for our Monte Carlo simulation is determined as *touchdown*. The touchdown criterion is due to the fact that our simulation model is relatively simple, and no surface feature is considered to describe complex bouncing motion of a CubeSat. Then, *success rate* describes the percentage of trajectories that touch down Didymoon surface over 1000 sample trajectories. Trajectories that do not touch down on the surface of either body over the course the simulation time are marked as *unsuccessful*.

It is now reasonable to investigate how individual sources, described in previous subsection, affects the success. Fig. 3 shows the results of individual sources in a Monte Carlo simulation for an example landing to the prime longitude. Recall that our analysis is restricted to equatorial trajectories.
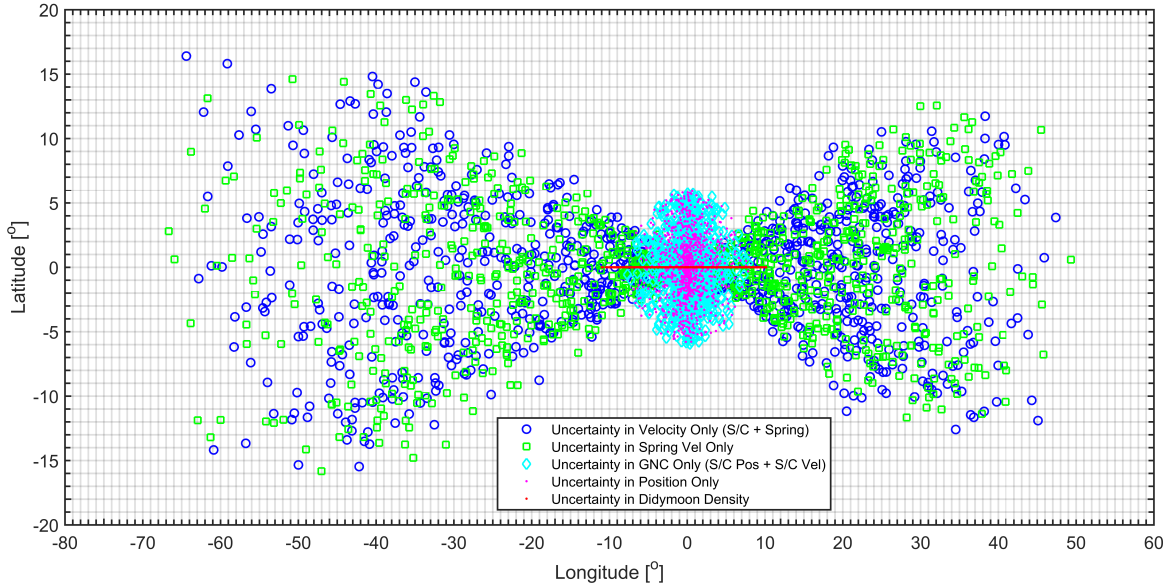
**Figure 3: The impact of individual sources on touchdown success.**

It is easily noticeable in Fig. 3 that spring errors have a dominating effect, which causes the largest spread by itself. (Note that spring errors also include angle error.) Particularly, spring errors cause the largest spread in both latitudinal and longitudinal direction. The "Butterfly-shaped" dispersion in Fig. 3 seems to be caused by the constrained landing geometry in local vertical. In this regard, the results here actually differ from some of the other studies that do not consider any specific landing geometry and obtain nominal trajectories directly in forward propagation [8, 12]. The combination of spring errors with GNC velocity errors makes a very little difference, although seems to increase the spread slightly when compared to spring-only errors. Assuming an ideal spring, GNC errors define an elliptic region of landings around the target longitude. When only position errors are considered in GNC system while everything else is nominal, the dispersion does not change much, although shrinks slightly in longitudinal direction. Finally, density-only effects show a longitudinal dispersion, as can be expected from a point-mass induced gravity model, of about $\pm 10^o$.

3.4. Results

3.4.1. Landing target at 0° latitude and 0° longitude

The first Monte Carlo simulation is applied to a landing location at 0° longitude and 0° latitude. This point is the closest point to L2 and the point of the lowest energy landings. First, the trajectory refining process is applied to the nominal trajectory, and the first intersection of the refined trajectory with the closest approach distance of the mothership ($r_{d,min}$) occurred at 239 m altitude above Didymoon surface. Then, a Monte Carlo analysis is carried out by applying the uncertainty models described previously and propagating the resultant sample of uncertain conditions forward in time. The success rate for this simulation is 99.9%, meaning that only one trajectory missed the surface or escaped before reaching it. The results can be seen in Fig. 4.

The dispersion shape is preserved compared to Fig. 3, suggesting that combined effect of all sources cannot diminish the effect of the spring itself. Although slightly more scattered, maximum longitudinal dispersion does not magnify by the addition of other effects and the maximum touchdown longitude stays around 65° longitude on the trailing side of Didymoon (negative longitudes) and about 50° longitude on the leading side (positive longitudes). This longitudinal dispersion seems to be in an agreement with MASCOT-2 requirements [22], and hence for AGEX, as it is proposed to be a "precursor" of MASCOT-2 [26]. This asymmetric longitudinal dispersion is closely associated with touchdown speeds on the surface. The grey "x" markers in Fig. 4 represent lower-than-average touchdown
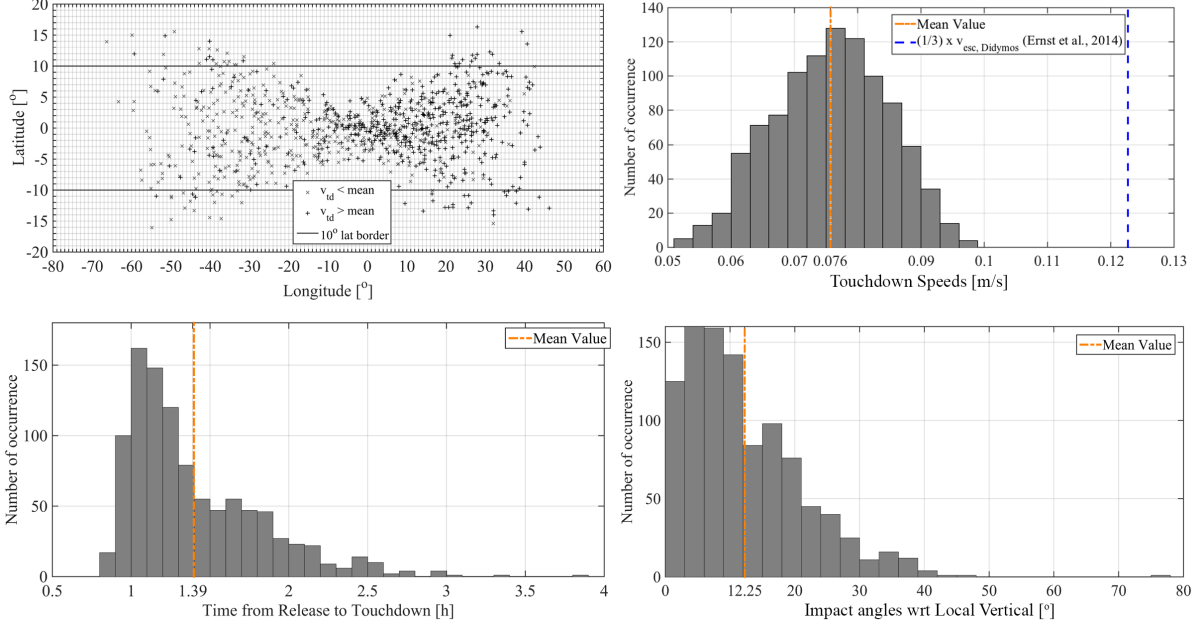
Figure 4: The results of Monte Carlo simulation for landings to 0° longitude.

speeds (hereafter, lower speeds) whereas the black "+" markers represent higher-than-average touchdown speeds (hereafter, higher speeds). Even though each color can be seen in both sides, the grey and the black markers are mainly populated on the trailing and leading sides, respectively. Obviously, those lower speeds are the result of lower energy trajectories. In a straightforward reasoning, it can be inferred that the dispersion stretches farther in the trailing side, because those trajectories simply take longer to the surface after the separation, hence uncertainties and errors (especially those associated with angles) propagate longer. A similar reasoning can also be applied to higher speeds. They mostly populate within 25° longitude from the nominal in the leading side, suggesting their higher speeds allow trajectory to reach the surface faster.

Compared to relatively wide and asymmetrical longitudinal variation, touchdown locations are in a narrower latitude range and almost symmetrical. All touchdowns occur roughly within $\pm 17^o$ latitudes. A vast majority, namely 91.3%, of trajectories touch down the surface in between $\pm 10^o$. Even though bouncing behavior of a CubeSat is rather unpredictable initially and heavily depends on touchdown conditions, it can be claimed that near-equatorial touchdowns would present a higher possibility to come to a rest within $\pm 60^o$ longitudes, which is defined to be maximum tolerable latitude for satisfactory illumination conditions for AGEX and MASCOT-2 [22, 26].

The results of touchdown speeds are presented in Fig. 4, in the upper right figure. Recall that the minimum vertical touchdown speed, $v_{landing}$ for this longitude is 5.81 cm/s, v_{L2} is 5.36 cm/s. Touchdown speeds are distributed roughly in the range between 5.5 cm/s to 10 cm/s, with their mean being 7.66 cm/s. Note in the figure the reference line at 12.3 cm/s, which shows one third of the estimated two-body escape speed of the Didymos system [27]. The maximum touchdown speed does not reach this point, suggesting that the CubeSat has a high chance to stay in the binary system after the touchdown.

In lower left corner of Fig. 4, time from release to touchdown is shown. As previously mentioned, the nominal trajectory reach the surface from the deployment altitude in ~1.2 h. The average time reach the surface is ~1.24 h, however relatively large number of trajectories reach the surface shorter than this, with the lowest being ~40 min. Those shorter trajectories are likely to be associated with the black "+" markers. In the other end of the figure, the time extends as long as 4 h, albeit with very low occurrence, which are likely to associated with lower speeds. It should be noted that resting of a CubeSat on the surface would take much longer than times shown here, as bouncing off the surface after touchdown is expected.

The last bar plot of Fig. 4 depicts impact angles in touchdown. That figure, in its present form, does not reveal much about touchdown conditions, as actual conditions strongly depend on surface properties and terrain. In this respect, it might even be preferable to land on shallower angles as comparing with vertical landing, if terrain has slopes. However, these results contain an important

10

information about trajectories itself, and the data can be interpreted in a different way. Since the landing geometry is defined in local vertical, amount of divergence from local vertical in touchdown may actually demonstrate the robustness of our trajectory design. The majority of touchdowns occur with impact angles within 15° with respect to local vertical. The maximum occurring impact angles are lower than the average value, 12.25^o. Higher impact angles are also observed, though in much lower occurrences, up to 50° for this case. Consequently, higher number of near-vertical landings in this Monte Carlo simulation suggests that the design of landing trajectory is relatively robust for at least this landing.

The simulation presented a very high success rate for d_{safe} = 200 m. However, it is reasonable to investigate greater close approach distances for the mothership in terms of touchdown success, as they are more preferable from risk assessment point of view for larger class missions. Table 3 provides the success rates of Monte Carlo simulation for various safe distances, d_{safe}, for the mothership, higher than 200 m.

Table 3: Success rates for various d_{safe}.

d_{safe}	Success rate
250 m	95.3%
300 m	76.1%
350 m	60.7%
400 m	57.1%

The results in Table 3 show a dramatic decrease in success rate as d_{safe} increases. The results of the dispersion shape, the speeds, the angles, and the duration, which are presented in Fig. 4, are not provided for each d_{safe}, but it is straightforward to infer that dispersions would become wider and time-to-touchdown increases with increasing d_{safe}. Impact speeds tend to increase, however still below one third of escape speed of the system. Impact angles are also still in near-vertical range, though number of occurrences of shallower angles increases.

All in all, Monte Carlo simulation for 0° latitude, 0° longitude shows a very high success rate at reasonably safe close approach distance for the mothership, and offers a successful landing prospect with relatively low speed. Moreover, these results can confidently be extended for regions in which trajectories present similar low-energy characteristics. It means then, that these results cover almost about one sixth of all equatorial region of Didymoon surface, as illustrated in Fig. 1. It has been demonstrated that for a successful touchdown to the lowest energy regions, trajectories need higher energies than their nominal. This might bring the discussion to bouncing behavior that is likely to occur. It is true that lower-speed landings are desirable to ensure to rest on the surface, but it apparently comes with an expense of risking the CubeSat not even reaching the surface, i.e. decreasing success rates. Furthermore, bounces may even be desirable in terms of mission success [26], as gravity science instruments generally require multi-point measurements. Additionally, shorter touchdown duration after separation is also within design requirements of AGEX [26] (i.e., 2 h), despite the expected duration for resting on the surface is longer. Impact angle results present a robust performance for our trajectory design under given assumptions and uncertainty sources presented. Finally, an increase in deployment altitude has a severely degrading impact on touchdown success, whose value decreases to almost its half when the altitude is only doubled.

3.4.2. Landings at other Longitudes

It has been concluded that the results presented in previous subsection can be extended to other nearby longitudes. However, the extent of this claim, at least for equatorial region in question here, needs to be justified. For this part of the analyses, the minimum close approach distance of the mothership has not been changed, i.e. d_{safe} = 200 m. Also, *CoR* value and trajectory refining constraints have not been modified. As the first intersection of a landing trajectory with the mothership distance is considered as the deployment location, landing trajectories that land on different longitudes will be deployed in different altitudes when measured from Didymos surface. This will of course have an impact on success rate as shown for the case in the previous section. The results of this analysis are provided in Table 4.

Table 4 shows the results of about 60°-wide area facing L2 point. In these results, an unexpected behavior is observed as the target longitudes extend from the prime longitude. It seems that, when longitudes are increasing through trailing side of Didymoon, success rates do not follow a continuous trend, i.e. decrease in success rates, as one can expect. It looks even more curious for example

Table 4: Results of Monte Carlo analysis in example landing targets.

| Lon.[^{o}]	Alt.[m]	S/R[%]	T/D Speed[cm/s]		T/D Angle[^{o}]		T/D Time[h]		T/D Lon.[^{o}]	
			Mean	Med	Mean	Med	Mean	Med	Mean	Med
+30	563	92.5	7.57	7.61	22.3	19.6	4.19	3.97	+149.3	+74.8
+20	352	81.5	7.44	7.47	26.4	24.3	2.41	2.19	+175.5	+106.9
+10	275	99.3	7.52	7.58	21.7	19.2	1.70	1.52	+167.6	+67.4
-10	220	99.8	7.64	7.64	8.01	6.17	1.30	1.17	-117.8	-26.4
-20	217	98.8	7.52	7.50	8.44	6.02	1.30	1.18	-30.0	-20.0
-30	210	96.1	7.47	7.48	12.5	7.00	1.39	1.24	-34.1	-28.6

longitude +30°, whose deployment altitude is the highest of all in Table 4, that performs much better than that of +20°, whose low-energy characteristics is closer to that of the prime longitude, and deployment altitude is much lower.

In both +20° and +30° cases, trajectories that miss the surface tend to perform a revolution around L2 point on the opposite side, exhibiting a dynamical behavior that very much resembles an incomplete Lyapunov orbit. Most of those incomplete revolutions intersect the distance, where Didymoon surface starts, for +30° case, which we define this intersection as touchdown. Those touchdowns seem to be the source of unexpected increase in the success rate. On the other hand, the same does not occur for landings to +20° longitude, i.e. revolutions generally grow smaller and escape the system in most cases. Figure 5 illustrates this behavior for +30° case; in which the arrow shows the forward propagation of the uncertain trajectory. Moreover, an evidence to this can also be found in Table 4, in which mean and median values of time-to-touchdown (designated as T/D time in the table) of +30° longitude are almost the twice that of +20° longitude, which is probably due to the time it takes to touchdown on the opposite side of the target longitude.
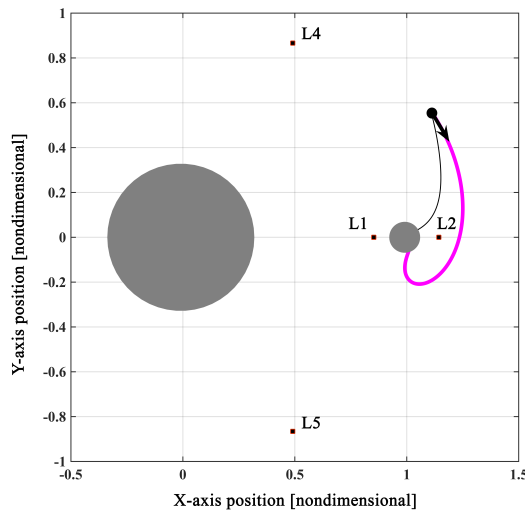
Figure 5: Incomplete revolution around L2 point.

Finally, Monte Carlo simulation for all equatorial targets can now be performed. In Fig. 5, target longitudes and deployment altitudes with their corresponding success rates, indicated by a color map, can be seen. In the figure, for instance, the deployment opportunity (i.e. the first intersection) for 0° longitude occurs at about 240 m altitude from Didymoon surface, and it results in a success rate between 90-100% as an estimate. Note the actual success rate is 99.9%. The diagonal texture in the middle represents longitudes where no deployment opportunities occur with the criteria explained previously. Recall that the cause of this is partially due to the choice of *CoR* = 0.7. Thus, it can be inferred that approximately half of the equatorial region is available for deployments with the provided criteria, albeit with varying success rates. Among them, approximately 60°-wide region in the L2-facing side present over 90% success with about half of them over 98%.
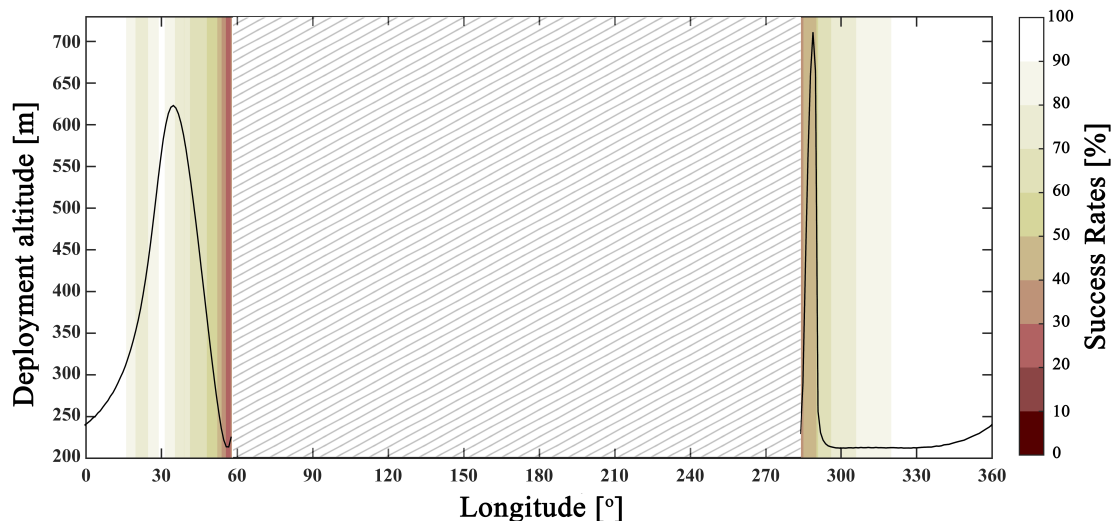
Figure 6: Overall Monte Carlo results for all target sites available.

Fig. 6 also demonstrates success rate trends associated to the unexpected behavior mentioned earlier. Around longitudes between 25°–35°, success rates do not follow a continuous trend and are increasing and decreasing again despite increasing deployment altitude. Around $+30^o$, the incomplete revolutions around L2 point result in more touchdowns on the opposite side of Didymoon than any other nearby target longitudes, hence higher success rates are observed, even though deployment altitudes are higher. The success rates on the trailing side show much more predictable behavior compared to that of in the leading side.

4. A Comment on Deployment Spring

As discussed earlier, the spring errors have the largest impact on success rates. Here, however, the spring has a rather hypothetical meaning. No specific deployment mechanism is considered, although an upper limit of 2 m/s is set to avoid excessively large deployment speeds. At the time of writing, AIM's deployment mechanism is designed to provide deployment speeds between 2–5 cm/s with a ±1 cm/s error [28]. In addition to this, Rosetta's deployment mechanism provided a push to Philae in the range of 5–50 cm/s with an emergency mechanism that is capable of 17 cm/s [21]. It is reasonable to see how the results here compare with those values. Nominal, minimum and maximum deployment speeds are estimated for landings to three target longitudes in the leading and the trailing sides and the prime longitudes, as shown in Table 5.

**Table 5: The spring velocities for three different longitudes.**

Lon [^{o}]	Nominal [cm/s]	Min [cm/s]	Max [cm/s]
0	8.22	7.76	8.69
20	7.95	7.46	8.45
350	8.20	7.75	8.63

The target longitude range in Table 5 exhibits similar landing characteristics; hence the longitudes in between or in their vicinity also have similar spring speeds. It has been already shown that lower speed deployments are prone to suffer from uncertainties and errors compared to higher speed deployments, due to the time duration to the surface.

The results of deployment speeds with our conservative *CoR* estimate fall more in the range of Rosetta's deployment mechanism than AIM's prospective one. It is true from our findings that lower speed deployments can be tolerated with lower *CoR* values. However, deployment mechanisms that provide extremely gentle pushes are likely to come at higher costs due to their precise machinery requirements. Thus, it seems that a deployment mechanism like Rosetta's might be a good fit to landing

13

requirements here, especially one considers its heritage. However, its adaptability to smaller size landers must be evaluated rigorously.

Another discussion point about the deployment spring is its magnitude error. Again, the deployment spring here is somewhat hypothetical, and it is assumed that a ±30% magnitude error would be conservative enough as 3σ error. In Monte Carlo simulation results, no other source but spring magnitude error clearly stood out as the main source of failed trajectories. Namely, almost all failed trajectories are observed to have spring magnitudes near the extremities in given error range. Figure 7 shows the failed trajectories for five cases with their corresponding spring magnitude errors.
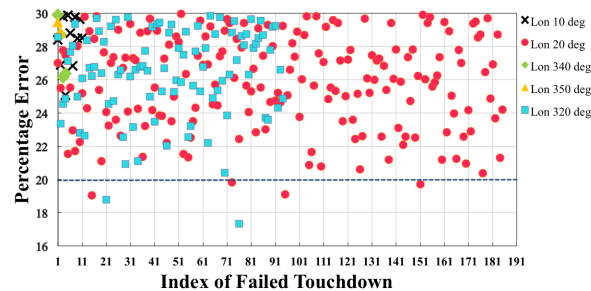
Figure 7: Percentage of spring magnitude errors for five landing targets.

It seems from Fig. 7 that, vast majority of failed trajectories have spring magnitude errors over 20%. It brings a clear inference, that lowering spring magnitude would increase success rates. However, the extent of increase is still uncertain, as it also depends on the spring angular error and other sources described earlier. Hence, a re-simulation was carried out with magnitude errors 20% for the same target longitudes. Even though our discussion is about a hypothetical spring, 20% magnitude error does not seem all that arbitrary. AIM's ISIPOD-derived CubeSat deployment mechanism is designed for dispersions on the order of 20%, and the measured dispersion was below 5% in engineering models [29]. Figure 8 presents the results of this analysis.
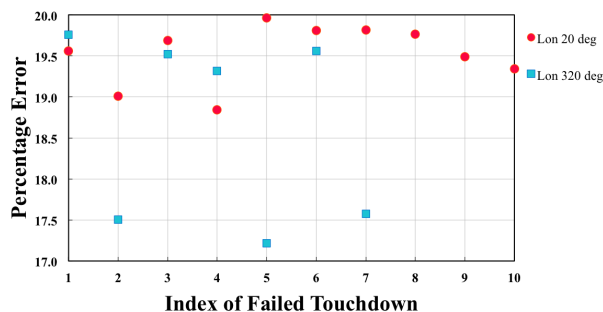
Figure 8: Percentage of spring magnitude errors after reducing the magnitude errors.

The analysis presents remarkable improvement in success rates. Out of five example cases, three of them resulted in 100% success. The success rates of the other two cases, namely 20° and 320° longitudes, improved from 81.5% to 99.9% and from 90.6% to 99.3%, respectively. However, in the first simulation, only a total of six failed trajectories have spring magnitude errors below 20%, whereas in the re-simulation, seventeen failed trajectories are observed below this value. This suggests, that either some of the sources that have been dominated by spring magnitude error become more effective after it is decreased, or success rates are within the accuracy limits of a Monte Carlo simulation with 1000 samples.

In general, it appears clear that an improvement in the deployment spring may greatly enhance the landing success, possibly not only for landing targets here, but a wider region in equator. The combination of that with lower angular errors would, not only increase success rates, but also reduce the touchdown dispersion area on the surface.

14

5. Conclusion

This paper has investigated the robustness of trajectories by means of a Monte Carlo simulation, to successfully send a CubeSat onto the surface of the smaller companion of Didymos. Building a model on top of the previously developed algorithm, various simulations have been carried out in order to assess statistical success of nominal trajectories, which are obtained in ideal conditions, under the effect of uncertainties and GNC errors. It is found, that the touchdown success is strongly related to deployment distance of the lander CubeSat, and the constrained landing geometry.

The backward integration technique is successfully utilized to obtain a nominal trajectory database. Several realistic, easily modifiable constraints are applied to refine the database to finally extract trajectories to be used in the simulation. It was found, that target low energy regions are considerably slow to reach surface, thus unavailable for shorter landing operations and prone to suffer from uncertainties. A simple, yet effective, scale-up process is applied to landing speeds in order to increase their energy by means of assuming a new, conservative coefficient of restitution, whose value is in harmony with observational findings and theoretical studies. This modification allowed a greater number of trajectories to be available for Monte Carlo simulation.

Realistically defined uncertainties and errors are added to refined trajectories and a sufficient number of trajectories is propagated to the surface in forward time. The results show, that for low energy regions present higher touchdown success rates than higher energy regions. However, higher success rates for low energy regions are strictly limited to low altitudes. Touchdowns mostly occur in near-equatorial latitudes, though with much wider longitudinal dispersion. It was found, that the dispersion shape on the surface is affected due to the constrained landing geometry, i.e. in local vertical, and in this respect it differs from some of the results in the literature. Impact speeds are always lower than escape speed of Didymos system. Impact angles are proven as a useful relative measure of robustness of trajectory design. Monte Carlo results for all equatorial longitudes show that high success rates are not limited to only few longitudes.

The results also helped to identify an unexpected behavior that have an impact on the results. Incomplete revolutions near L2 point triggers an irregular success rate change for some of the longitudes in the leading side of Didymoon. Furthermore, the analysis on deployment spring shows, that separation speeds for Didymoon mainly fall in in the range that Rosetta's deployment mechanism is capable of. Although that may be a good fit to the requirements here, its adaptability to smaller landers need to be evaluated rigorously. Finally, a reduction is considered the magnitude error of the deployment spring, which is consistent with the existing mechanism considered for AIM, and the success is enhanced greatly. This remarkable result suggests that degrading effects of higher altitudes may in fact be mitigated by an improvement in separation mechanisms.

To conclude, it should be noted that the Monte Carlo analyses carried out here only represent the statistical success rates of the local vertical landings, designed in the backwards integration approach. Different landing conditions may exhibit more successful deployment conditions. Similarly, an extension of the simulation into a spatial may also reveal more regions to be reached with higher statistical success. It should also particularly be noted that these results are not conclusive and as accurate as the simulation model, nonetheless, this fact does not attenuate the relevance and importance of the outcomes.

References

[1] J. L. Margot, M. C. Nolan, L. A. M. Benner, S. J. Ostro, R. F. Jurgens, J. D. Giorgini, D. B. Campbell, Binary asteroids in the near-Earth object population, Science 296 (2002) 1445–1448.

[2] M. A. Barucci, A. F. Cheng, P. Michel, L. A. M. Benner, R. P. Binzel, P. A. Bland, M. Zolensky, MarcoPolo-R near earth asteroid sample return mission, Experimental Astronomy 33 (2012) 645–684.

[3] R. C. Anderson, D. Scheeres, S. Chesley, the BASiX Science Team, A Mission Concept to Explore a Binary Near Earth Asteroid System, in: Proceedings of the 45th Lunar and Planetary Science Conference, The Woodlands, Texas. March 17–21, 2014. Paper number 1777.

[4] A. F. Cheng, J. Atchison, B. Kantsiper, A. S. Rivkin, A. Stickle, C. Reed, S. Ulamec, Asteroid Impact and Deflection Assessment mission, Acta Astronautica 115 (2015) 262–269.

[5] J. P. Sanchez, C. Colombo, Impact hazard protection efficiency by a small kinetic impactor, Journal of Spacecraft and Rockets 50 (2013) 380–393.

[6] A. G. I. Carnelli, R. Walker, Science by Cubes: Opportunities to Increase AIM Science Return, in: Proceedings of the 4th Interplanetary CubeSat Workshop, London, UK. May 27–28, 2015. Paper number 2015.B.3.1.

[7] N. M. B. R. O. Karatekin, D. Mimoun, N. Gerbal, The Asteroid Geophysical EXplorer (AGEX) to Explore Didymos, in: Proceedings of the 5th Interplanetary CubeSat Workshop, Oxford, UK. May 28–29, 2016. Paper number 2016.A.2.1.

[8] S. Tardivel, D. J. Scheeres, Ballistic Deployment of Science Packages on Binary Asteroids, Journal of Guidance, Control, and Dynamics 36 (2013) 700–709.

[9] S. Tardivel, P. Michel, D. J. Scheeres, Deployment of a lander on the binary asteroid (175706) 1996 FG$_3$, potential target of the european MarcoPolo-R sample return mission, Acta Astronautica 89 (2013) 60–70.

[10] S. Tardivel, C. Lange, S. Ulamec, J. Biele, The Deployment of MASCOT-2 to Didymoon, in: Proceedings of the 26th AAS/AIAA Space Flight Mechanics Meeting, Napa, California. February 14–18, 2016. Paper number AAS 16-219.

[11] S. Tardivel, Optimization of the Ballistic Deployment to the Secondary of a Binary Asteroid, Journal of Guidance, Control, and Dynamics 39 (2016) 2790–2798.

[12] F. Ferrari, Non-Keplerian Models for Mission Analysis Scenarios about Small Solar System Bodies, Ph.D. thesis, Politecnico di Milano, 2015.

[13] O. Celik, J. P. Sanchez, Opportunities for Ballistic Soft Landing in Binary Asteroids, Journal of Guidance, Control, and Dynamics (2017). Ahead of print.

[14] S. Tardivel, D. J. Scheeres, P. Michel, S. van Wal, P. Sanchez, Contact Motion on Surface of Asteroid, Journal of Spacecraft and Rockets 51 (2014) 1857–1871.

[15] S. Sawai, J. Kawaguchi, D. J. Scheeres, N. Yoshikawa, M. Ogasawara, Development of a Target Marker for Landing on Asteroids, Journal of Spacecraft and Rockets 51 (2014) 1857–1871.

[16] T. Kubota, S. Sawai, T. Hashimoto, J. Kawaguchi, Collision dynamics of a visual target marker for small-body exploration, Advanced Robotics 51 (2014) 1857–1871.

[17] V. Szebehely, Theory of Orbits, Academic Press: New York, 1967.

[18] Y. Ren, J. Shan, A novel algorithm for generating libration point orbits about the collinear points, Celestial Mechanics and Dynamical Astronomy 120 (2014) 57–75.

[19] E. Canalias, A. Blazquez, E. Jurado, T. Martin, Philae Descent Trajectory Computation and Landing Site Selection on Comet Churymov-Gerasimenko, in: Proceedings of 23rd International Symposium on Spaceflight Dynamics, Pasadena, California. Oct 29 – Nov 2, 2012. Paper number GC-2.

[20] S. Ulamec, C. Fantianti, M. Maibaum, K. Geurts, J. Biele, S. Jansen, L. O'Rourke, Rosetta Lander–Landing and Operations on Comet 67P/Churyumov–Gerasimenko, Acta Astronautica 125 (2016) 80–91.

[21] J. Biele, S. Ulamec, M. Maibaum, R. Roll, L. Witte, E. Jurado, P. Munoz, W. Arnold, H.-U. Auster, C. C. et al., The Landing(s) of Philae and Inferences About Comet Surface Mechanical Properties, Science 349 (2015) 1–6.

[22] T. Ho, J. Biele, C. Lange, AIM MASCOT-2 Asteroid Lander Concept Design Assessment Study, Technical Report, German Aerospace Center (DLR), 2016.

[23] H. Yano, T. Kubota, H. Miyamoto, T. Okada, D. Scheeres, Y. Takagi, K. Yoshida, M. Abe, S. Abe, O. Barnouin-Jha, Touchdown of the Hayabusa Spacecraft at the Muses Sea on Itokawa, Science 312 (2006) 1350–1353.

[24] D. Pignatelli, Poly Picosatellite Orbital Deployer Mk. III Rev. E User Guide, 2014.

[25] E. S. A. (ESA), Asteroid Impact Mission: Didymos Reference Model, 2015. Last Access: April 12, 2017.

[26] O. Karatekin, B. Ritter, D. Mimoun, N. Murdoch, A. Cadu, J. Carrasco, J. G. Quiros, H. Vassuer, V. Larock, S. Tardivel, N. Rambaux, S. Ranvier, J. deKeyser, M. Yyseboodt, V. Dehant, N. Gerbal, SysNova COPINS Asteroid Geophysical Explorer: AGEX Challenge Analysis Draft Final Report, Technical Report, Royal Observatory of Belgium, 2016.

[27] C. M. Ernst, O. S. Barnouin, A. M. Stickle, Analytical Calculations of Ejecta Mass and Crater Size Produced by the Impact of the DART Spacecraft into the Moon of Didymos, in: Proceedings of 1st AIDA International Workshop, Laurel, Maryland. October 15–17, 2014.

[28] R. Walker, D. Binns, I. Carnelli, M. Kueppers, A. Galvez, CubeSat Opportunity Payload Intersatellite Network Sensors (COPINS) on the ESA Asteroid Impact Mission (AIM), in: Proceedings of the 5th Interplanetary CubeSat Workshop, Oxford, UK. May 24–25, 2016. Paper number 2016.B.1.2.

[29] C. Bernal, LV-POD Executive Summary Report Issue 1.1, Technical Report, Innovative Solutions in Space, 2016.